Notes

Bull. Korean Chem. Soc. **2011**, Vol. 32, No. 2   705
DOI 10.5012/bkcs.2011.32.2.705

Application of Long-range-corrected Density Functional in Metallated Porphyrin Analogues for Dye-sensitized Solar Cells

Mannix P. Balanay, Sang Hee Lee, Soo-Chang Yu, and Dong Hee Kim*

*Department of Chemistry, Kunsan National University, Gunsan 573-701, Korea. *E-mail: dhkim@kunsan.ac.kr*
Received July 16, 2010, Accepted November 29, 2010

The basic composition of a dye-sensitized solar cell (DSSC) involves semiconductor (usually TiO_2), redox electrolyte, counter electrode, and sensitizer. The sensitizer, which is chemically adsorbed on the TiO_2 surface, is mainly responsible for the photoelectronic properties of the solar cell. Most of the researches are focused in the design of a sensitizer that can achieve the highest solar cell efficiency. As to date, Ru-based sensitizers are still the highest performing dye, with an efficiency reaching up to 11.4%,[1] followed closely by the organic-based sensitizers, with a highest efficiency of 10.3 %.[2] The basic structure of the dye contains a donor-(π-conjugated bridge)-acceptor (D-π-A) system, which should be properly tailored to attain desirable properties of the dye, such as the highest occupied molecular orbital (HOMO) must be located below the redox couple of the electrolyte and the lowest unoccupied molecular orbital (LUMO) is situated above the conduction band edge level of TiO_2; there should be an efficient unidirectional charge transfer between the donor and acceptor moiety; and the dye should be able to absorb most of the radiation of the solar light, especially at the visible and near-IR regions.[3]

With the advent of new and faster computers, the theoretical design of a sensitizer could not only lead to faster optimization process but also drastically decrease the operational cost in the synthesis of such sensitizers. One of the parameters involved in the optimization of the dye is its ability to absorb light, thus it is necessary to accurately model the absorption spectrum of the dye by using proper theoretical methodology. Most of the excited state calculations involving DSSC sensitizers used time-dependent density functional theory (TDDFT) with the B3LYP[4,5] exchange-correlation (xc) functional. However, the performance of B3LYP and other currently used xc functionals do not correctly describe the distance coordinate (R) in the charge transfer (CT) state between the positive and negative charges at large distances from an atom or a molecule.[6,7] This interaction decays faster than 1/R and is often ascribed to an electron-transfer self-interaction error.[8,9] These functionals fail to provide accurate estimations of excited state energies in molecules with extended π-conjugation and CT capability, features normally present in DSSC sensitizers.[6-9] Researchers have used various methods to address these shortcomings, by applying an asymptotically corrected xc potential,[10] varying the percentage of Hartree-Fock exchange in the xc functionals,[11] using linear scaling techniques,[12,13] or employing range-separated functionals, such as the long-range corrected (LC) functional[14-16] and Coulomb-attenuating methods.[17,18] Among these methods, the range-

separated functionals have attracted much attention since they exhibit the correct asymptotic distance dependence and removal of the spurious, low-energy CT states that usually contaminates the TDDFT calculations for those compounds having CT and extended π-conjugated properties.[6,7]

In this study, a comparison between the commonly used functional, B3LYP and the LC technique (LC-BLYP), introduced by Hirao and co-workers[14-16] were performed to test the effectivity of the LC functional in the calculation of excited state energies in TDDFT framework of β-substituted Zn porphyrin analogues (Figure 1). The difference between these two functionals is that, in the LC scheme, long-range electron-electron interactions were combined with the HF exchange integral, which was then divided into short- and long-range components. The pure density functional (i.e. BLYP) which was modified according to the LC scheme is defined as[14-16]

$$E_{LC-DFT} = \left(-\frac{1}{2} \sum_\sigma \int \rho_\sigma^{4/3} K_\sigma \left\{ 1 - \frac{8}{3} a_\sigma \left[\sqrt{\pi} erf\left(\frac{1}{2a_\sigma}\right) + 2a_\sigma \left(b_\sigma - c_\sigma\right) \right] \right\} d^3R \right)$$
$$+ \left(-\frac{1}{2} \sum_\sigma \sum_i^{occ} \sum_j^{occ} \iint \psi_{i\sigma}^*(r_1) \psi_{j\sigma}^*(r_1) \times \frac{erf(\omega r_{12})}{r_{12}} \psi_{i\sigma}(r_2) \psi_{j\sigma}(r_2) d^3r_1 d^3r_2 \right) + E_c^{DFT}$$

(1)

where, ρ_σ is the density of σ-spin electrons at a spatial point r, K_σ contains the gradient correction as defined in the exchange functional used, $a_\sigma = \omega K_\sigma^{1/2}/6\sqrt{\pi}\rho_\sigma^{1/3}$, $b_\sigma = \exp(-1/4 a_\sigma^2) - 1$, $c_\sigma = 2a_\sigma^2 b_\sigma + 1/2$, $r_{12} = |r_1 - r_2|$ is the absolute distance between electrons at coordinate vectors r_1 and r_2, $\psi_{i\sigma}$ is the ith σ-spin orthonormal molecular orbital, and ω is an adjustable damping parameter having units of inverse length which determines the balance of DFT and HF exchanges or the short-range and long-
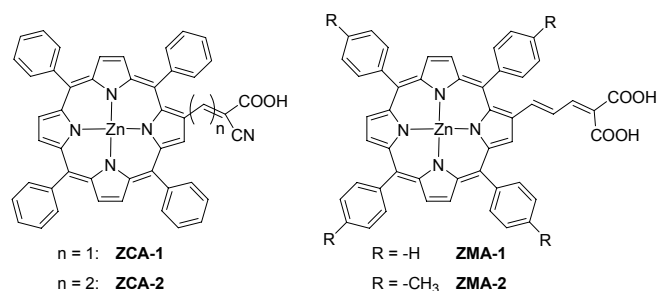

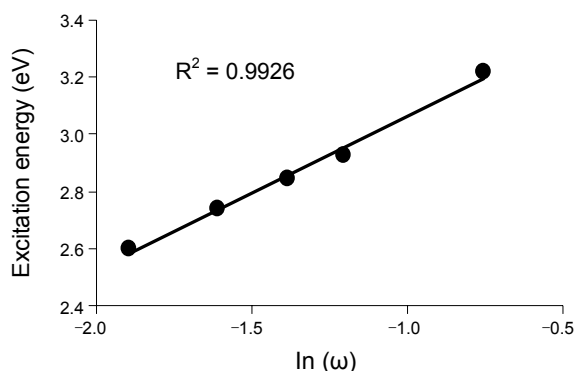**Figure 1.** Structures of Zn tetraarylporphyrin analogues.

Figure 2. Vertical excitation energies of the maximum oscillator strength as a function of the natural logarithm of the damping parameter, ω, for **ZCA-2** calculated at TD-LC-BLYP/6-31G(d)//B3LYP/6-31G(d) in THF using CPCM framework.

range parts at intermediate r_{12}, and E_c^{DFT} is the DFT correlation functional (LYP), The first term in eqn. 1 accounts for the short-range interaction, while the second term accounts for the long-range interaction. For $\omega = 0$, it reproduces the original exchange functional. On the other hand, setting $\omega = \infty$, results to the standard HF calculation. In contrast to the LC technique, the B3LYP functional simply mixes the conventional exchange functional and the HF exchange at a fixed ratio, independent of electron-electron distances.[15]

The damping parameter in the LC scheme is dependent on the type of electronic structure. For example, in coumarin, anthracene, and pyridazine analogues, the optimized damping parameter ranges from 0.17 to 0.20 Bohr^{-1}, while for smaller molecules such as carbon monoxide and acetaldehyde the damping parameter reaches up to 0.90 Bohr^{-1}.[19,20] To find the appropriate damping parameter for the molecules in consideration, we simulate the ω-dependence of the singlet-singlet vertical excitation energy of the maximum oscillator strength of **ZCA-2** with a damping parameter range of $0.15 \leq \omega \leq 0.47$ Bohr^{-1}.

As shown on Figure 2, the excitation energies undergoes a hypsochromic shift when the damping parameter was increased. Based on the graph obtained in Figure 2, we used the equation of the line (Excitation energy = ln(ω)0.447 + 3.457) to estimate the appropriate damping parameter given the experimental λ$_{max}$ of the system which is 2.66 eV[21] of **ZCA-2**. It gave a damping parameter of 0.17 Bohr^{-1} which enables the short-range coulomb operator to fully decay to zero on the length scale of the molecule.[19] For the rest of the molecules, a damping parameter of 0.17 Bohr^{-1} in the LC scheme was used to calculate the excited state energies.

The computed vertical excitation energies together with their oscillator strengths using LC-BLYP xc functionals are shown in Tables S1-S4 (supplementary information). It shows that the LC-BLYP and the B3LYP xc functionals reproduced qualitatively the expected trend that the excitation energies decreases as the degree of π-conjugation increases. The close analogy between the excited state energies of **ZMA-1** and **ZMA-2** confirms that the substitution of a methyl group at the *para*-position of the *meso*-phenyl rings of the porphyrin macrocycle has minimal effect on the band positions. Nevertheless, the substitution caused the excited state energies to be slightly red-shifted
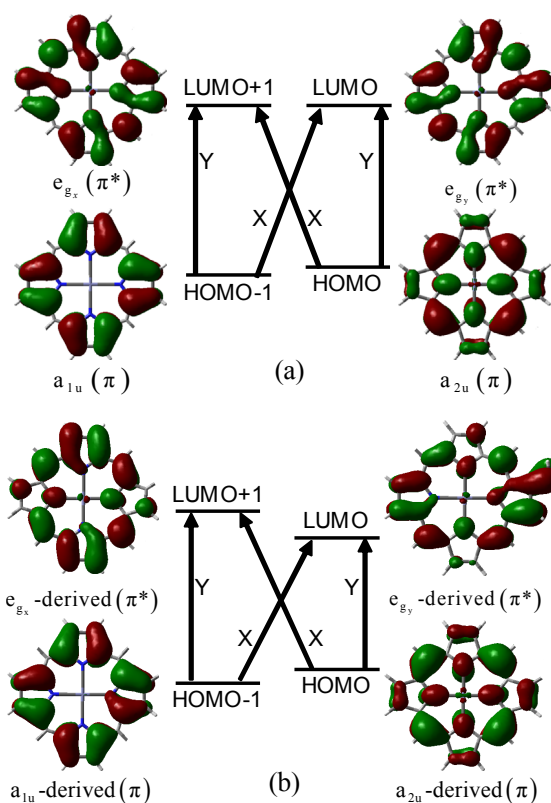

Figure 3. Schematic orbital energy diagram showing one-electron excitation states that corresponds to the transition states of (a) zinc tetraphenylporphyrin and (b) β-substituted zinc tetraarylporphyrin. The phenyl rings and the β-substituents are removed to emphasize the molecular spatial orientation of the porphyrin macrocycle.

confirming the increased electron donating capacity of **ZMA-2** than **ZMA-1**.[22,23] A comparison between different acceptor moieties having the same donor and linker groups shows that, for both functionals, a large bathochromic shift was observed for the analogue containing cyanoacetic acid (**ZCA-2**) when compared to the analogue with malonic acid as the acceptor moiety (**ZMA-1**). The large bathochromic shift was likely due to the higher electron-withdrawing capability of the cyanoacetic acid than malonic acid.[23]

Typically, porphyrins absorb strongly in the visible range of 400 - 700 nm, which is divided into two main distinct bands: the single intense Soret (B)-band (400 - 450 nm) and the multiple weak Q-bands (500 - 700 nm). The contributing molecular orbital (MO) transitions at these bands, for the analogues in consideration, arises from π-π* transitions involving four molecular orbitals as predicted by Gouterman.[24] Figure 3 shows the electronic states responsible for the singlet excitations involving the four MOs (HOMO-1, HOMO, LUMO, and LUMO+1) of Zn tetraphenylporphyrin (ZnTPP) and the β-substituted Zn tetraarylporphyrins. The change of the electronic structure when ZnTPP was added with a β-substituent introduces only very minimal effect of MOs of the porphyrin macrocycle. The results showed that the shapes of the electron densities of the β-substituted porphyrin for the four-molecular orbitals are very similar to ZnTPP, which one could infer that the MOs of the β-substituted porphyrins are derived from the MOs of ZnTPP.[22] This
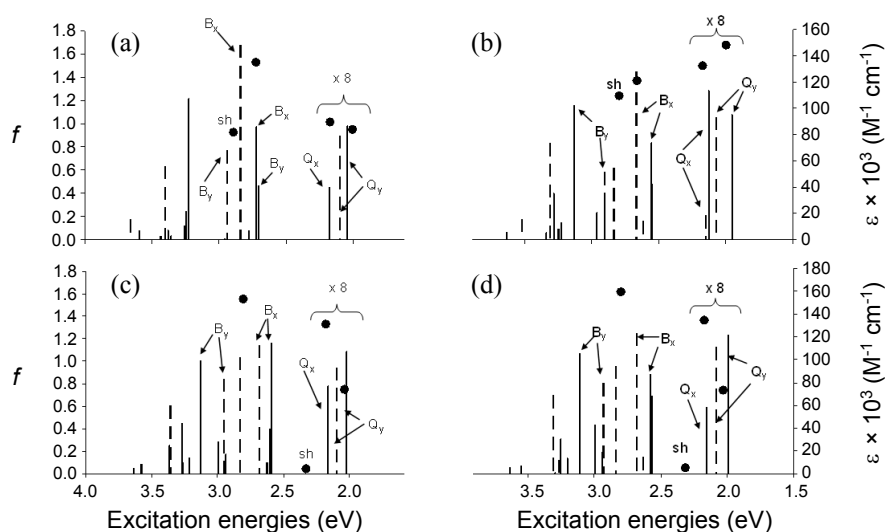
Figure 4. Comparative schematic optical spectrum of (a) **ZCA-1**, (b) **ZCA-2**, (c) **ZMA-1**, and (d) **ZMA-2** based on B3LYP (solid line) and LC-BLYP with $\omega = 0.17$ Bohr^{-1} (dashed line). Circular bullets indicate the experimental absorption peaks from references 21 and 26.

could help assign the transition states of the β-substituted system to provide a simple interpretation of the Zn porphyrin spectra based on Gouterman's four-orbital model. The Q_y state would mostly undergoes a HOMO → LUMO transition, while a HOMO-1 → LUMO transition would be observed for a Q_x state. The B-band region, though mostly seen as one peak, is a combination of two intense perpendicularly polarized electronic transitions (B_x and B_y) which was confirmed from polarization measurements.[25] The B_x and B_y states usually undergo HOMO → LUMO+1 and HOMO-1 → LUMO+1 transitions, respectively (see supplementary information for the MO assignment of the transition states). It should be noted that the existence of a relative mixing of these four orbitals in each transition, including a strong contribution of LUMO+2 orbital at the B-band region, could influence the oscillator strengths and energy states of the analogues. The relative position of the transition states based on the energy levels in Figure 3 could be generally arranged in a decreasing energy pattern of $B_y > B_x > Q_x > Q_y$.

Figure 4 illustrates schematically the resulting positions and corresponding states of the transitions energies of zinc porphyrin analogues using B3LYP and LC-BLYP xc functionals. The calculation of LC-BLYP was done with a 0.17 Bohr^{-1} damping parameter. As observed in Figure 4, the correlations between the experimental[21,26] and theoretical approach using the different xc functionals were dependent on specific band regions of the porphyrin analogues. Nevertheless, both xc functionals depicted the correct trend of transitions states ($B_y > B_x > Q_x > Q_y$) except for **ZCA-1** calculated with B3LYP xc functional, where it places the B_y state lower in energy than the B_x state.

Analysis of the individual transition states indicated that for the Q_y-band, the long-range functional deviates from the experimental values by 0.10 eV for **ZCA-1** and about 0.07 eV for the analogues with extended π-conjugation (**ZCA-2**, **ZMA-1**, and **ZMA-2**), whereas smaller deviations of 0.01 to 0.04 eV were observed for the B3LYP functional for all analogues. This shows

that the LC-BLYP approach was more sensitive to those analogues with extended π-conjugation but still overestimated the excitation energies compared to the B3LYP values. As for the Q_x-band, the differences between the LC-BLYP and the B3LYP functionals were negligible compared to experimental results.

The two intense, polarized transitions at the B-band were properly depicted for both xc functionals, however the amount of splitting between these transitions are dependent with the xc functional used (Figure 4). Splitting values of about 0.10 and 0.25 eV were observed for **ZCA-1** and for those analogues with extended π-conjugation (**ZCA-2**, **ZMA-1**, and **ZMA-2**), respectively, when calculated with the long-range functional. However, when the B3LYP xc functional was used, a 0.02 eV splitting value was observed for **ZCA-1,** while the average splitting value for the analogues with extended π-conjugation was at 0.55 eV. The very small splitting value observed for **ZCA-1** when calculated with the B3LYP functional could be due to the spurious positioning of the B_y transition that was situated lower than the B_x transition as mentioned above. And the reason for the larger splitting between the B-band transitions when analogues were calculated with the B3LYP xc functional was the existence of multiple lower intensity transitions between the B_x and B_y transitions. Analysis of the MO orbitals involved in the lower intensity states gave transitions of HOMO-2 → LUMO and HOMO-3 → LUMO that were often assigned to the N-band which is usually located higher in energy than the B-band.[27] This mixing was also observed with other porphyrin analogues with a D-π-A system using the TD-B3LYP method.[6] This greatly affects the quality and accuracy of the calculated B-band transition energies when compared to experimental results. When calculating the amount of difference between the experimental and theoretical results at the B-band region, where the two B-band transitions were calculated based on a weighted mean procedure, it was found that when dealing with extended π-conjugated molecules, LC-BLYP provided a more consistent deviation from the experimental data ranging from 0.01 eV to 0.07 eV, however B3LYP produces deviations of up

to 0.23 eV. For the **ZCA-1** analogue, the B3LYP xc functional provided a closer correlation a difference of 0.01 eV compared to 0.15 eV for LC-BLYP. However, the discrepancy on the position of the B_y component also needs to be taken into account. This clearly shows that a more realistic depiction of the excitation energies at the B-band were observed when the energies are calculated with the long-range corrected functional than the common hybrid functional (B3LYP).

In conclusion, for low-lying transition states (Q-bands), the B3LYP xc functional provides a better correlation with the experimental results. But, LC-BLYP and B3LYP produced the same trend in excitation energies, with the LC-BLYP only slightly blue-shifted compared to the B3LYP xc functional. However, at the B-band region, due to the mixing of the N-bands between the two B-band transitions in B3LYP calculations, the LC-BLYP xc functional provides a better choice in the calculation of excited state energies of porphyrin analogues, especially those containing extended π-conjugation. Overall, taking into account the errors of the B3LYP functional at the B-band region, the LC-BLYP xc functional gave a better depiction of the excitation energies of the sensitizers for dye-sensitized solar cells, especially for extended π-conjugated analogues.

Computational Details

The ground state geometries of **ZCA-1**, **ZCA-2**, **ZMA-1**, and **ZMA-2** optimized at B3LYP/6-31G(d) *in vacuo* were recovered from references 22 and 23. The lowest 10 singlet excitation energies were computed based on TDDFT formalism using B3LYP and LC-BLYP functionals with 6-31G(d) basis set. The effect of solvation was considered using conductor-like polarized continuum model (CPCM) framework.[28,29] Tetrahydrofuran (THF) and *N,N*-dimethylformamide (DMF) were used as solvents for **ZCA** and **ZMA** analogues, respectively.

TD-B3LYP results from the references were not used due to the differences in the default model type and dielectric constants used in the CPCM calculations in Gaussian 09 giving slight differences in values. The use of the same theoretical parameters in CPCM calculations also provides consistencies in the analysis of results when compared to LC-BLYP calculations.

All TDDFT calculations were done using Gaussian 09 package.[30] The contributions of the excited state configurations to each transitions were calculated using SWizard program.[31]

References

1. Cao, Y.; Bai, Y.; Yu, Q.; Cheng, Y.; Liu, S.; Shi, D.; Gao, F.; Wang, P. *J. Phys. Chem. C* **2009**, *113*, 6290-6297.
2. Zeng, W.; Cao, Y.; Bai, Y.; Wang, Y.; Shi, Y.; Zhang, M.; Wang, F.; Pan, C.; Wang, P. *Chem. Mater.* **2010**, *22*, 1915-1925.
3. Grätzel, M. *Inorg. Chem.* **2005**, *44*, 6841-6851.
4. Becke, A. D. *J. Chem. Phys.* **1993**, *98*, 5648.
5. Lee, C.; Yang, W.; Parr, R. G. *Phys. Rev. B* **1988**, *37*, 785-789.
6. Cai, Z. L.; Crossley, M. J.; Reimers, J. R.; Kobayashi, R.; Amos, R. D. *J. Phys. Chem. B* **2006**, *110*, 15624-15632.
7. Jacquemin, D.; Perpete, E. A.; Scalmani, G.; Frisch, M. J.; Kobayashi, R.; Adamo, C. *J. Chem. Phys.* **2007**, *126*, 144105-144112.
8. Dreuw, A.; Head-Gordon, M. *J. Am. Chem. Soc.* **2004**, *126*, 4007-4016.
9. Dreuw, A.; Head-Gordon, M. *Chem. Rev.* **2005**, *105*, 4009-4037.
10. Tozer, D. J.; Handy, N. C. *J. Chem. Phys.* **1998**, *109*, 10180-10189.
11. Sancho-Garcia, J. C. *Chem. Phys.* **2007**, *331*, 321-331.
12. Yam, C.-Y.; Zheng, X.; Chen, G. *J. Comput. Theor. Nanosci.* **2006**, *3*, 857-863.
13. Champagne, B.; Guillaume, M.; Zutterman, F. *Chem. Phys. Lett.* **2006**, *425*, 105-109.
14. Tawada, Y.; Tsuneda, T.; Yanagisawa, S.; Yanai, T.; Hirao, K. *J. Chem. Phys.* **2004**, *120*, 8425-8433.
15. Chiba, M.; Tsuneda, T.; Hirao, K. *J. Chem. Phys.* **2006**, *124*, 144106-144111.
16. Iikura, H.; Tsuneda, T.; Yanai, T.; Hirao, K. *J. Chem. Phys.* **2001**, *115*, 3540-3544.
17. Yanai, T.; Tew, D. P.; Handy, N. C. *Chem. Phys. Lett.* **2004**, *393*, 51-57.
18. Cohen, A. J.; Mori-Sanchez, P.; Yang, W. *J. Chem. Phys.* **2007**, *126*, 191109-191105.
19. Wong, B. M.; Cordaro, J. G. *J. Chem. Phys.* **2008**, *129*, 214703-214708.
20. Rohrdanz, M. A.; Herbert, J. M. *J. Chem. Phys.* **2008**, *129*, 034107-034109.
21. Wang, Q.; Campbell, W. M.; Bonfantani, E. E.; Jolley, K. W.; Officer, D. L.; Walsh, P. J.; Gordon, K.; Humphry-Baker, R.; Nazeeruddin, M. K.; Grätzel, M. *J. Phys. Chem. B* **2005**, *109*, 15397-15409.
22. Balanay, M. P.; Kim, D. H. *J. Mol. Struct.:THEOCHEM* **2009**, *910*, 20-26.
23. Balanay, M. P.; Kim, D. H. *Curr. Appl Phys.* **2011**, *11*, 109-116.
24. Gouterman, M. *J. Mol. Spectrosc.* **1961**, *6*, 138-163.
25. Shkirman, S. F.; Solov'ev, K. N.; Kachura, T. F.; Arabei, S. A.; Skakovskii, E. D. *J. Appl. Spectrosc.* **1999**, *66*, 68-75.
26. Campbell, W. M.; Jolley, K. W.; Wagner, P.; Wagner, K.; Walsh, P. J.; Gordon, K. C.; Schmidt-Mende, L.; Nazeeruddin, M. K.; Wang, Q.; Grätzel, M.; Officer, D. L. *J. Phys. Chem. C* **2007**, *111*, 11760-11762.
27. Sekino, H.; Kobayashi, H. *J. Chem. Phys.* **1987**, *86*, 5045-5052.
28. Cossi, M.; Rega, N.; Scalmani, G.; Barone, V. *J. Comput. Chem.* **2003**, *24*, 669-681.
29. Balanay, M. P.; Kim, D. H. *Phys. Chem. Chem. Phys.* **2008**, *10*, 5121-5127.
30. Frisch, M. J.; Trucks, G. W.; Schlegel, H. B.; Scuseria, G. E.; Robb, M. A.; Cheeseman, J. R.; Scalmani, G.; Barone, V.; Mennucci, B.; Petersson, G. A.; Nakatsuji, H.; Caricato, M.; Li, X.; Hratchian, H. P.; Izmaylov, A. F.; Bloino, J.; Zheng, G.; Sonnenberg, J. L.; Hada, M.; Ehara, M.; Toyota, K.; Fukuda, R.; Hasegawa, J.; Ishida, M.; Nakajima, T.; Honda, Y.; Kitao, O.; Nakai, H.; Vreven, T.; Jr., J. A. M.; Peralta, J. E.; Ogliaro, F.; Bearpark, M.; Heyd, J. J.; Brothers, E.; Kudin, K. N.; Staroverov, V. N.; Keith, T.; Kobayashi, R.; Normand, J.; Raghavachari, K.; Rendell, A.; Burant, J. C.; Iyengar, S. S.; Tomasi, J.; Cossi, M.; Rega, N.; Millam, J. M.; Klene, M.; Knox, J. E.; Cross, J. B.; Bakken, V.; Adamo, C.; Jaramillo, J.; Gomperts, R.; Stratmann, R. E.; Yazyev, O.; Austin, A. J.; Cammi, R.; Pomelli, C.; Ochterski, J. W.; Martin, R. L.; Morokuma, K.; Zakrzewski, V. G.; Voth, G. A.; Salvador, P.; Dannenberg, J. J.; Dapprich, S.; Daniels, A. D.; Farkas, Ö.; Foresman, J. B.; Ortiz, J. V.; Cioslowski, J.; Fox, D. J., Gaussian 09, Revision B.1, Gaussian, Inc., Wallingford CT, 2010.
31. Gorelsky, S. I., SWizard program, Version 4.6, University of Ottawa, Canada, 2010, http://www.sg-chem.net/swizard.